Structural Safety of Photovoltaic Modules in the Building Envelope

C. Hemmerle

Technical University of Munich, Center for Sustainable Building, Germany, claudia.hemmerle@tum.de

The mechanical performance of photovoltaic modules has not been adequately characterized for use as glazing product in the building envelope. As a result, the modules are subject to individual approval by the building authorities in many building-integrated applications. This paper presents experimental research on glass based photovoltaic modules, analyzing their mechanical properties in comparison with regulated construction products. The focus is on the influence of photovoltaic thin-film coatings on the bending strength of the float glass used as a substrate or superstrate and on the post-breakage behavior of glass-glass modules. The four-point bending test according to EN 1288-3 was modified in terms of specimen dimensions in order to test full-size photovoltaic glass panes. The modified set-up was verified as a suitable and simple test method to determine and confirm strength values. Edge ablation was found to reduce glass strength rather than the PV coating and cell scribing processes, but the reduction is less than 10 % and the minimum strength value of float glass can still be met. Residual strength testing of glass-glass photovoltaic modules in different load and temperature scenarios showed that the integration of crystalline silicon cells as well as thin-film solar cells improves the post-breakage behavior of glazings. A critical point may be mechanical failure within the layers of thin-film cells on glass associated with the potential danger of broken glass pieces falling down. Standard glass-glass module configurations appear to provide the same or higher residual strength performance as laminated safety glass, if the interlayer material is approved for use in laminated safety glass.

Keywords: Photovoltaics, bending strength, residual strength, four point bending, approval, laminated safety glass

1. Introduction

Integrating photovoltaic (PV) systems into their envelope can improve sustainability of buildings. The majority of the PV modules used for building integration contains glass as cover and backing material and thus can be classified as laminated glass. In various European countries, many glazing applications require the use of laminated safety glass. As a result, building-integrated PV modules are subject to individual approval in many cases, because the mechanical performance has not yet been adequately characterized (DIBt 2012). A growing number of national technical approvals granted in Germany demonstrates that glass-glass PV modules are generally able to provide structural safety equivalent to laminated safety glass.

Glass-glass PV modules basically differ according to laminated glass with embedded PV cells – whether it be crystalline silicon wafer cells or thin-film cells as a coating on polymer substrates – and thin-film cells as a coating directly deposited on one of the two glass panes. Since most requirements equally apply to the majority of PV modules of a specific technology, general assessment and regulation is desirable. This research provides systematic experimental results on the mechanical performance of PV modules.

Residual strength testing of glass-glass photovoltaic modules aims to characterize residual load-bearing capacity of the three most relevant PV module configurations compared to laminated safety glass and to identify the relevant influence parameters as well as adequate test scenarios. The three configurations are glass-glass modules with silicon wafer cells, thin-film cells on glass superstrate and thin-film cells on flexible polymer substrate.

A second research focus is on the influence of photovoltaic thin-film coatings on the bending strength of the float glass used as a substrate. The product standards define minimum values of the bending strength of different glass products. While crystalline PV modules use regular glass products with well-known mechanical strength properties according to harmonized product standards, the bending strength of coated glass must be confirmed by the manufacturer. The influence of the thin-film coating processes on the bending strength of the float glass used as substrate or superstrate glass has not yet been sufficiently investigated. Deposition temperatures, laser scribing and edge ablation to pattern and isolate the PV cells might result in residual stresses or surface defects that are critical for final glass strength (Dietrich 2013). A modified four point bending test method using full-size PV glass panes as specimens is introduced as a simple method to determine and confirm the bending strength of PV thin-film on glass products.

2. Bending strength of PV coated glass

2.1. Determination of the bending strength of glass

The practical bending strength of glass primarily depends on the surface quality, on the glazing geometry and on the type of loading. Thus, strength of glass is not a material constant, but a statistical value associated with a particular probability of breakage under particular test conditions. For glass in building, it is determined by destructive testing according to EN 1288. Experimentally determined strength values strongly depend on the size and edge quality of the test specimens as well as on the homogeneity of the applied stress. Due to the cutting process, the edges of glass usually are particularly fragile. Therefore, EN 1288 offers three test methods for flat glass aimed at different objectives. The edge quality or the intended application may serve as selection criteria.

Four point bending (EN 1288-3) includes effects of the edges and allows to determine two different values of bending strength: for the strength of the surface area including the edges (overall strength) or for the separate strength of the edges (edge strength). The test method is primarily suitable for thermally toughened glass. In contrast, coaxial double ring tests only consider the surface area. There are two set-ups: one with large test surface areas measuring 0.24 m^2 (EN 1288-2) and one with small test surface areas of 113 or 254 mm^2 (EN 1288-5).

2.2. PV products and the modified test method

The coaxial double ring method with large test surface areas is more appropriate for determining characteristic values as the basis for designing than the coaxial double ring test with small test surface, which leads to large scattering of the strength values and is rather recommended for comparative evaluation (EN 1288-1), e. g. in factory production control. Yet, the standardized specimen size of 1000 mm x 1000 mm assigned to the large test surface is not manufacturable in many typical thin-film PV production facilities tailored to standard module sizes of, for example, 1200 mm x 600 mm. Moreover, testing the comparatively thin glass panes (typically 3.2 mm) used for thin-film PV is hardly manageable. A modified ring size between the two test standards could be used, but neither testing geometry nor evaluation procedure are standardized and non-homogenous stress distribution due to the large deflections and geometrical nonlinearities has to be considered. Another important argument against the double ring test is the circumferential edge ablation of the PV glasses after the coating process, which is presumed to most significantly influence the bending strength. The ablated areas nearby the edges cannot be located inside the coaxial double ring test surface.

A problem with testing PV thin-film glass panes in four point bending is that coating and edge ablation of 1100 mm x 360 mm specimens as defined in EN 1288-3 is extremely demanding. Cutting the coated panes, however, would manipulate the test results, because the cutting process damages the surface at the edges and leads to breakage at lower stresses. In addition, the edge ablation would be missing at the cut edge.

In order to avoid these practical problems of the standardized test methods, a four point bending test equipment has been modified to be able to test full-size PV thin-film glass panes with original edges. PV panes of two different PV manufacturers using different technologies and dimensions were analyzed in comparison with thermally toughened glass panes in the standard specimen width of 360 mm. These two thin-film technologies include cadmium telluride (CdTe) and micromorphous silicon (a-Si/μ-Si) PV cells on glass superstrate, which means that the PV coated glass pane serves as cover glass in the ready-made PV module.

The modification was to extend the specimen width from 360 mm to 600, 1100 and 1300 mm. The slightly altered specimen length is negligible. All other test parameters and the principle remained the same: the specimens are placed between two support rollers 1000 mm apart. Two bending rollers 200 mm apart apply an increasing force until the glass breaks. Additionally, glass panes without PV coating but only with TCO (transparent conductive oxide = electrical front contact) inline coating were used as reference to investigate the effect of the PV coating.
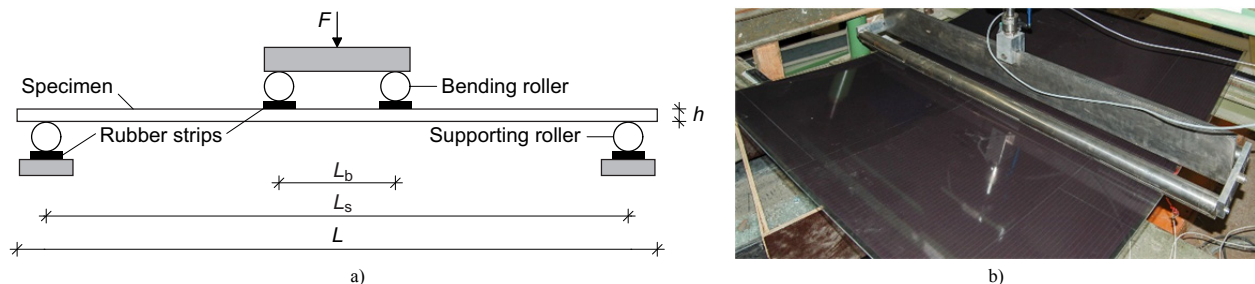
Fig. 1a) Principle of the four point bending test method and b) test equipment with 1100 mm wide PV-coated specimen.
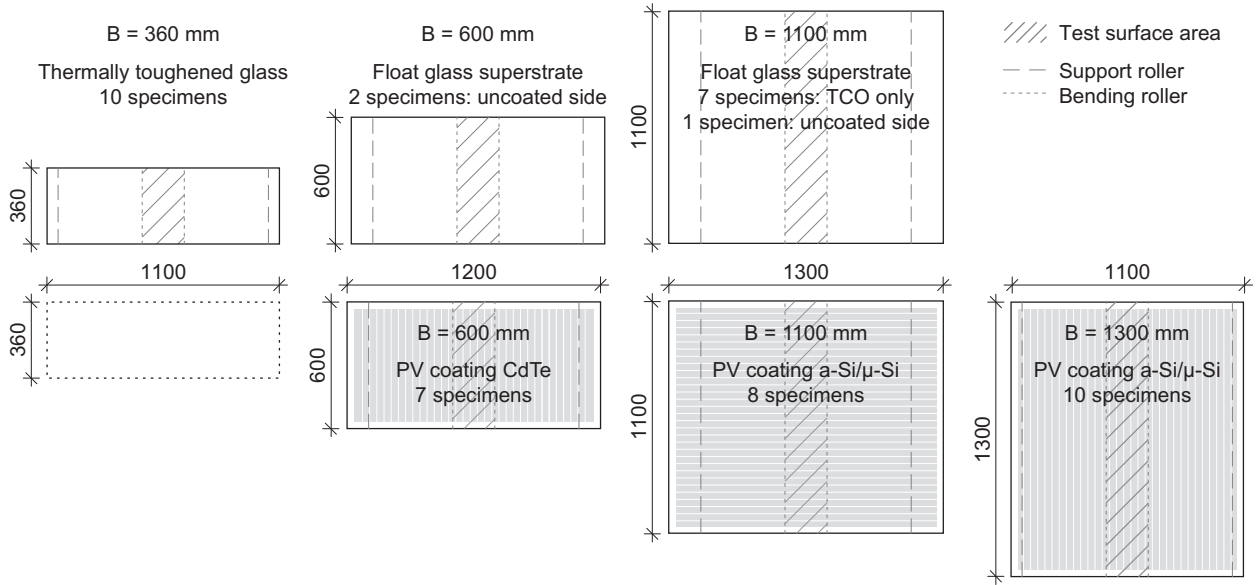
Fig. 2 Standard-size thermally toughened glass specimens and modified specimen widths.

Using the linear beam theory, the induced tensile stress leading to breakage σ_{bB} can be approximated from the maximum force during failure F_{max} and the contribution of the self-weight σ_{bG}.

$$\sigma_{bB} = \sigma_{bth}\left(F_{max}\right) = F_{max}\frac{3\left(L_s - L_b\right)}{2Bh^2} + \sigma_{bG} \tag{1}$$

where

σ_{bB}	Bending strength
σ_{bth}	Bending stress calculated from the linear beam theory
F_{max}	Maximum force, fracture load
L_s	Distance between the center lines of the supporting rollers
L_b	Distance between the center lines of the bending rollers
B	Specimen width
h	Specimen thickness
σ_{bB}	Bending stress imposed by the self-weight of the specimen

The beam theory assumes the stresses in the tested surface area are uniformly distributed and constant. In reality, a secondary transverse curvature around the longitudinal axis and membrane effects occur. Therefore, the relationship between bending force and stresses is not linear. The longitudinal tensile stresses vary significantly over the test area and increase from the center towards the edges of the specimen.
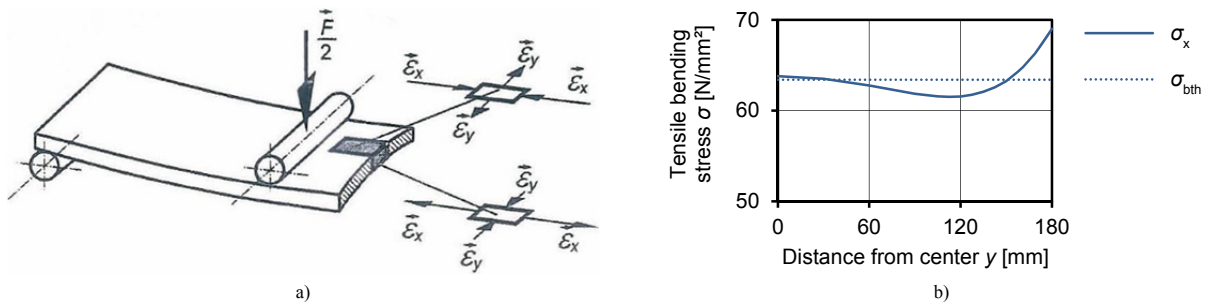
Fig. 3a) Secondary curvature of a specimen under four point bending (Blank et al. 1994); b) actual, non-uniform longitudinal bending stress σ_x versus linearly calculated stress according to simple beam theory σ_{bth} at a load corresponding to $\sigma_{bth} = 63.4$ N/mm^2.

For this reason, EN 1288-3 modifies the bending stress according to the beam theory σ_{bth} to a strength value called effective stress σ_{eff} by applying a factor k analyzed by Blank et al. (1994). σ_{eff} represents a weighted mean value homogeneously acting on the test surface area with the same probability of failure as the real, non-uniform stress.

$$\sigma_{bB} = \sigma_{eff}\left(F_{\max}\right) = k \cdot \sigma_{bth}\left(F_{\max}\right) = k \cdot \left(F_{\max} \frac{3\left(L_s - L_b\right)}{2Bh^2} + \sigma_{bG} \right)$$

(2)

where

σ_{eff} Effective bending stress
k Dimensionless factor for calculation of the effective bending stress
       $k = k_s$ when all the fractures are included to determine the overall strength
       $k = k_e$ when only edge fractures are included to determine the edge strength

With larger specimen width, the test surface area increases and thus, due the so-called size effect described by Blank et al. (1990; 1994), the probability that it contains a critical surface defect increases. In addition, the distribution of the tensile strength values changes due to the different geometrical conditions. Thus, the assessment of the factor k and its standard value $k_s = 1$ for a conservative determination of the surface area strength might no longer apply to the large and thin PV specimen. In order to analyze the validity of equation (2) for the modified four point bending, the standard-size specimen as well as those with extended width were equipped with three strain gauges along the transverse axes.
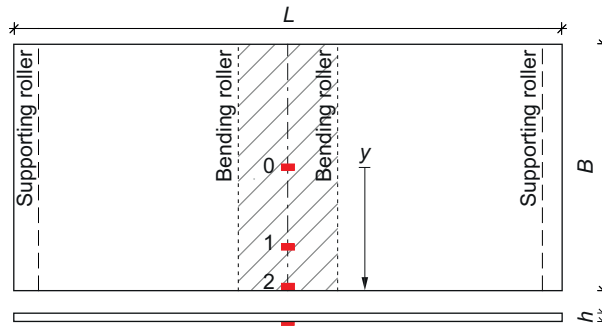
Fig. 4 Position of the strain gauges along the axis.

The longitudinal strains measured on three points (see figure 4) serve to verify numerical calculations performed simultaneously. If the model shows sufficient accuracy, it can be used to analyze the tensile bending stresses developing in the specimens with modified widths during four-point bending.

2.3. Numerical results

The stress development across the different widths of the specimens was analyzed using the geometrically non-linear calculation method of the SJ Mepla 3.5.9 finite element software for structural glass design. The calculated stresses refer to the center of the strain gauges with 1.57 mm grid width. Figure 5 shows the results at different loads for two of the four specimen widths analyzed.
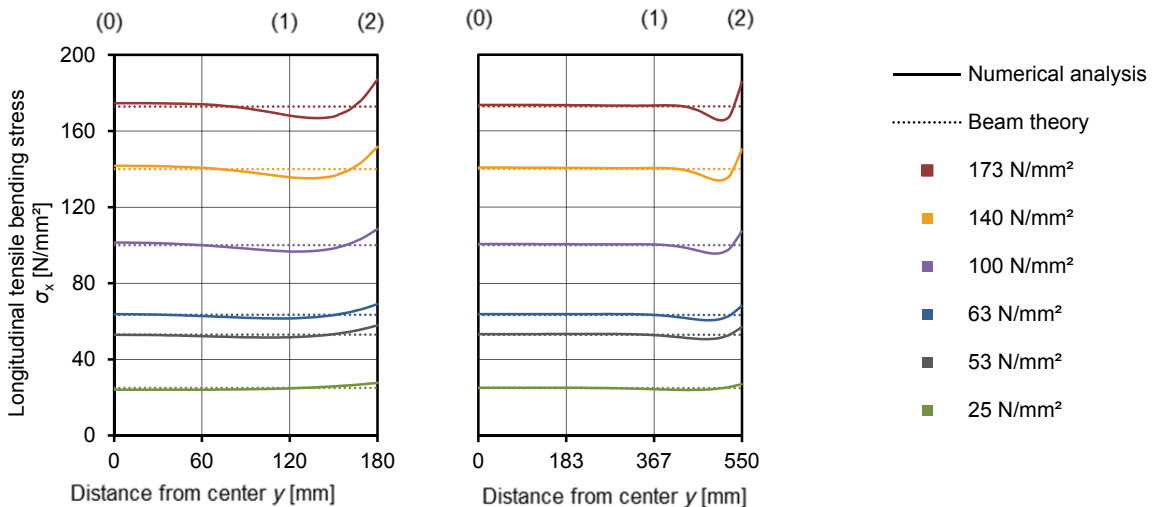
Fig. 5 Longitudinal tensile stresses across the specimen width along the transverse axis at bending stresses σ_{bth} between 25 and 173 N/mm².
Left: $B = 360$ mm, right: $B = 1100$ mm. Glass thickness $h = 3.2$ mm, Young's modulus $E = 70 \cdot 10^3$ N/mm², Poisson's ratio $\nu = 0.23$.

With increasing specimen width as well as with increasing load, the variation of the strain as well as the tensile bending stresses reduce, in particular the peak values at the edges (2) decrease (see table 1).

Table 1: Development of the relative peak strains and stresses at the edges (2) with increasing specimen width B at different loads.

σ_{bth}	$B = 360$ mm		$B = 600$ mm		$B = 1100$ mm		$B = 1300$ mm	
	$\varepsilon_L(2) / \varepsilon_{th}$	$\sigma_L(2) / \sigma_{bth}$	$\varepsilon_L(2) / \varepsilon_{th}$	$\sigma_L(2) / \sigma_{bth}$	$\varepsilon_L(2) / \varepsilon_{th}$	$\sigma_L(2) / \sigma_{bth}$	$\varepsilon_L(2) / \varepsilon_{th}$	$\sigma_L(2) / \sigma_{bth}$
53 N/mm^2	107.7 %	107.7 %	106.1 %	106.2 %	106.2 %	106.3 %	106.0 %	106.1 %
63 N/mm^2	107.3 %	107.4 %	105.9 %	106.0 %	106.0 %	106.1 %	105.8 %	105.8 %
100 N/mm^2	106.7 %	106.7 %	105.3 %	105.4 %	105.6 %	105.7 %	105.4 %	105.4 %
140 N/mm^2	106.2 %	106.3 %	104.9 %	105.0 %	105.4 %	105.5 %	105.1 %	105.2 %
173 N/mm^2	105.9 %	106.0 %	104.6 %	104.8 %	105.3 %	105.3 %	104.9 %	105.0 %

2.4. Experimental results

A transparent self-adhesive film was affixed to the specimens holding the glass fragments together to be able to locate the fracture origins. While the thermally toughened glass specimens failed at the edge in 9 of 10 cases, the fracture origin of the wider TCO or uncoated-side specimens more often lay in the interior of the surface area (6 cases) than at the edges (4 cases). In contrast to the TCO specimens, the PV specimens of identical edge quality showed breakage from the edge in 24 of 25 cases. No correlation with the cells' laser patterning was found.
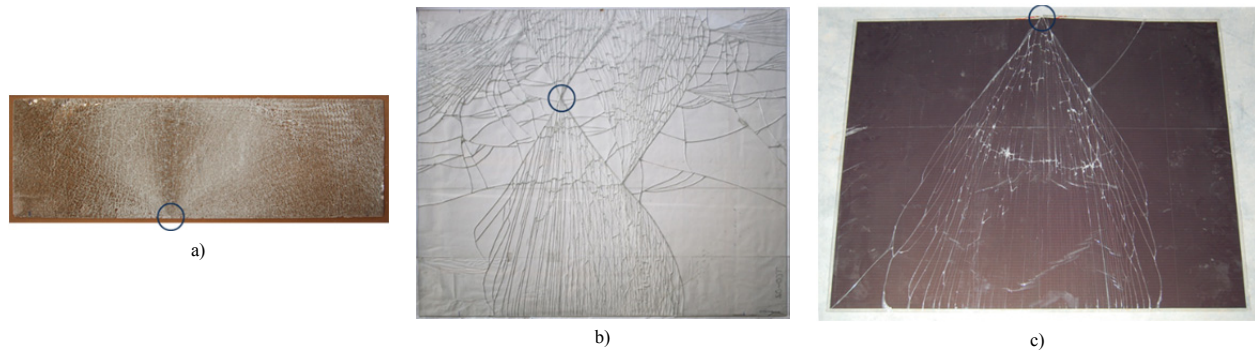
Fig. 6 Examples of fracture patterns and origins of a) standard-size thermally toughened glass, b) TCO, c) horizontal PV a-Si/µ-Si specimens.

The longitudinal strains measured during the experiments were used to calculate the related longitudinal tensile stresses using the individual thickness of each specimen which was determined as the arithmetic mean of measurements on four points. The results confirmed the reduced maximum stresses at the edges with increasing specimen width (see table 2). Table 2 also shows that the simulation model underestimates the increase of tensile stresses towards the edge to a higher degree for the standard specimen width of 360 mm and to a lesser extent with increasing width. Thus, the extended specimen widths actually result in a more considerable reduction of stress at the edges and improve homogeneity of the bending stress even more than the results of the numerical calculations reveal. In general, the calculations agree very well with the measured values over the whole range of specimen sizes and loads showing deviations between -3 % and +4 % (see table 3). Each measured value incorporates a series of 6 to 15 averaged measurements.

Table 2: Measured relative peak strains at the edges (2) with increasing specimen width B at different loads.

σ_{bth}	$B = 360$ mm	$B = 600$ mm	$B = 1100$ mm	$B = 1300$ mm
	$\varepsilon_L(2) / \varepsilon_{th}$	$\varepsilon_L(2) / \varepsilon_{th}$	$\varepsilon_L(2) / \varepsilon_{th}$	$\varepsilon_L(2) / \varepsilon_{th}$
53 N/mm^2	111.2 %	108.6 %	106.2 %	105.7 %
63 N/mm^2	110.4 %	107.8 %	105.5 %	105.3 %
100 N/mm^2	109.3 %			
140 N/mm^2	108.3 %			
173 N/mm^2	107.9 %			

Table 3: Deviation of the numerically calculated longitudinal strain from the measured values at $\sigma_{bth} = 63$ N/mm^2.

Measuring point	$B = 360$ mm	$B = 600$ mm	$B = 1100$ mm	$B = 1300$ mm
0	+1.3 %	+4.1 %	+0.8 %	+0.7 %
1	+3.0 %	+0.7 %	+0.1 %	-0.3 %
2	-2.8 %	-1.8 %	+0.5 %	+0.4 %

Table 4 shows the results of the four point bending tests applying equation (1). The center deflections w are normalized to the specimen thickness h. The standard-size thermally toughened glass specimens failed at loads referring to an average theoretical bending stress $\sigma_{bth} = 176$ N/mm². Most specimens were still unbroken and thus delivered strain values up to a value of 173 N/mm². Being float glass, the PV and TCO specimens broke at lower stresses with σ_{bth} mostly between 63 and 80 N/mm². For the expanded widths, the maximum stress at the edges is already below 108 % of σ_{bth} at this low bending stress level, whereas for the original specimen size the peak stress at the edges fall below 108 % not until load reaches the fracture level of thermally toughened glass (see table 2). As a result, the proposed modification improves the applicability of the four point bending test method to float glass.

Table 4: Results of photovoltaic glasses in four point bending.

Specimens	number of specimens considered	B [mm]	h [mm] mean value	σ_{bth} [N/mm²] mean value	σ_{bth} [N/mm²] standard deviation	w/h
TCO	4	1100	3.16	74.3	4.5	20,0
PV CdTe	4	600	3.21	68.0	5.9	17,8
PV a-Si/µ-Si longitudinal	8	1100	3.14	69.2	4.0	19,1
PV a-Si/µ-Si transversal	8	1300	3.16	69.7	1.3	18,4

2.5. Evaluation procedure

Due to the very good agreement between numerical and experimental results, the numerical calculations can be used to analyze the tensile bending stresses with modified specimen width and to evaluate possible variations of the factor k_s. Determining the overall bending strength of the surface area including the edges requires the use of the factor k_s. Blank et al. (1994) provide k_s for 360 mm wide specimen assuming a Weibull exponent $\beta = 5$ (figure 7b)). Figure 7a) shows the calculated stress development of the three widths analyzed in comparison to the 360 mm standard width at a theoretical bending stress $\sigma_{bth} = 63$ N/mm² near the fracture level of float glass. According to the diagram, larger specimen widths result in a more uniform stress development across the specimen width. The range of the stress drop becomes narrower and moves near the edge. Most importantly, the maximum stress at the edge decreases. These results correspond with the strain measurements, which exhibited even more severe reduction at the edges, as discussed above. They also agree with the observed fracture origins, which with increasing specimen width did not predominantly lie at the edge any more.
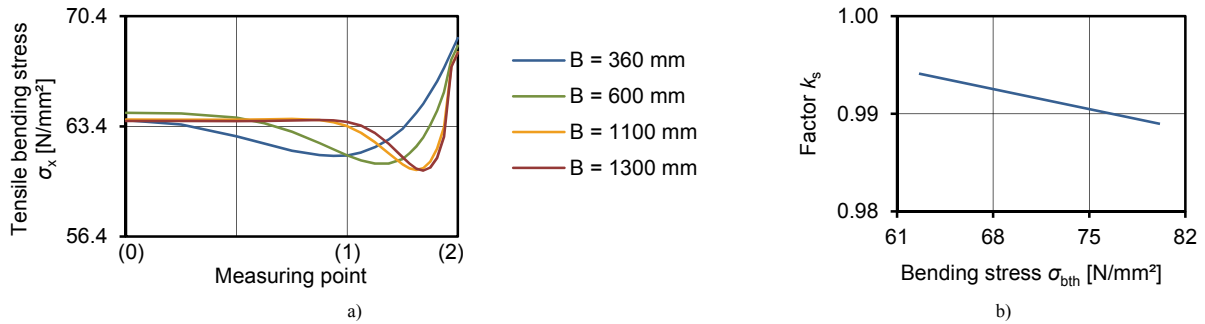
Fig. 7a) Numerically calculated longitudinal tensile stresses at a theoretical bending stress $\sigma_{bth} = 63.4$ N/mm²; b) Factor k_s for specimen thickness 3.2 mm interpolated from Blank et al. (1994).

In order to evaluate the stress level, equation (3) was used to calculate the effective stress σ_{eff} at a theoretical bending stress $\sigma_{bth} = 63.4$ N/mm² corresponding to the fracture level of PV coated float glass.

$$\sigma_{eff} = \left[\frac{1}{A_K} \cdot \int_{A_K} \sigma_I{}^\beta \, dA_K \right]^{\frac{1}{\beta}}$$

(3)

where

A_K Test surface area
σ_I Greater principal tensile stress at the test surface area
β Weibull exponent

The effective stress σ_{eff} incorporates the Weibull exponent β, which is determined from statistical interpretation of the testing series, to consider the probability of flaws and the flaw distribution. Figure 8 shows the calculated effective stress σ_{eff} and the respective values of k_s determined using $k_s = \sigma_{bth} / \sigma_{eff}$, which can be derived from

equation (2), for different values of β. The influence of the Weibull exponent on σ_{eff} and factor k_s decreases with larger specimen widths. As a result, factor k_s remains very close to 1 although the scattering of the strength values tends to decrease and the Weibull exponent tends to increase with larger test surface areas.
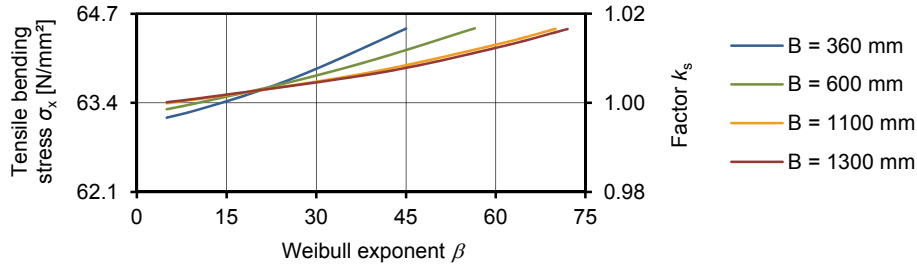
Fig. 8 Effective bending stress values and resulting factor k_s at $\sigma_{bth} = 63.4$ N/mm^2 as a function of the Weibull exponent.

In addition, the influence of the size effect must be taken into account. Because of the higher probability of critical defects in larger test surface areas, fracture occurs at lower load. In order not to underestimate the strength of the glass specimens, the determined bending strength requires correction. Derived from Weibull statistics, the size effect on glass strength is described by the relationship between the size of two different surface areas and two different principal tensile stresses, which act uniformly on these areas and lead to the same probability of their fracture (Blank et al. 1990). Transferred to the modified specimen width in four point bending, equation (4) considers the size effect at constant distance between the bending rollers $L_b = 200$ mm. As a result, effective bending strength values must be corrected by +2 to +6 % (see table 5) to be on a par with the test standard level.

$$\frac{\sigma_{eff}(A_{K,2})}{\sigma_{eff}(A_{K,1})} = \left(\frac{A_{K,1}}{A_{K,2}}\right)^{\frac{1}{\beta}} = \left(\frac{L_{b,1} \cdot B_1}{L_{b,2} \cdot B_2}\right)^{\frac{1}{\beta}} = \left(\frac{B_1}{B_2}\right)^{\frac{1}{\beta}}$$

(4)

Table 5: Weibull exponent and resulting correction factor for the effective bending stress in order to incorporate the increased test surface areas.

	$B = 360$ mm	$B = 600$ mm	$B = 1100$ mm (TCO)	$B = 1100$ mm (PV)	$B = 1300$ mm
β	32.2	9.8	23.5	18.5	63.7
$\sigma_{eff,corr} / \sigma_{eff}$	1.00	1.05	1.05	1.06	1.02

Table 6 determines the overall bending strength values of the PV and TCO specimens using factor k_s as a combination of figure 7b) and 8 and the correction factor from table 5 to incorporate the size effect.

Table 6: Calculation and correction of the overall bending strength in the surface area, including the edges (mean values, standard deviation in brackets).

Specimens	B [mm]	σ_{bth} [N/mm^2]		k_s		σ_{eff} [N/mm^2]		$\sigma_{bB} = \sigma_{eff,corr}$ [N/mm^2]	
TCO	1100	74.3	(4.5)	0.995	(0.001)	74.0	(4.3)	77.6	(4.6)
PV CdTe	600	68.0	(5.9)	0.994	(0.002)	67.6	(5.7)	71.2	(6.1)
PV a-Si/μ-Si longitudinal	1100	69.2	(4.0)	0.996	(0.001)	68.9	(3.9)	73.2	(4.1)
PV a-Si/μ-Si transversal	1300	69.7	(1.3)	1.007	(0.000)	70.2	(1.3)	71.7	(1.4)

For the PV specimens, however, the fact that all specimens broke from the ablated areas at a distance of not more than 12 mm from the edge requires to discuss whether the evaluation procedure to determine the overall bending strength is applicable. On one hand, the test results do not characterize the bending strength in the coated areas, where no failure occurred. Thus, the actual bending strength in the unbroken coated areas is higher than the results in table 6 imply. On the other hand, bending stresses in the ablated area are supposed to be higher than the weighted average across the entire test surface area and the calculated overall bending strength will underestimate the glass strength in the ablated area. Therefore, the edge ablation area is analyzed separately.

Figure 9 provides an approach for factor k_e and a factor k_{e12} to describe the relative stress at both limits of the ablated area right at the edge and 12 mm from the edge as a function of the relative center deflection in the style of EN 1288-3. The curves were derived from the numerical and experimental results. At the fracture level of the PV specimens, the factors range from 1,043 to 1,090 in the case of the specimen width 600 mm and from 0,992 to 1,072 in the case of 1100 and 1300 mm. The application of equation (3) within the limits of the ablated areas resulted in a factor k_{ea} to calculate the effective bending strength in the edge ablation area. Here, a variation of the Weibull exponent β has no significant influence.
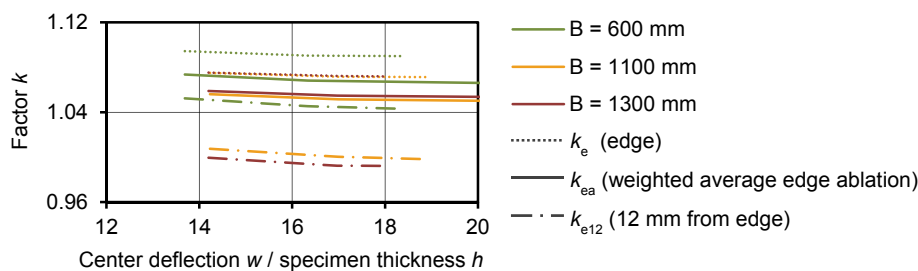
Fig. 9 Maximum and minimum level of the bending stress in the area of edge ablation and weighed average factor k_{ea} for the effective bending strength. With $\beta = 9.8$ for $B = 600$ mm, $\beta = 18.5$ for $B = 1100$ mm and $\beta = 63.7$ for $B = 1300$ mm.

The effective bending strength of the edge ablation area reaches about 73 N/mm² for both PV technologies and exceeds or insignificantly falls below the overall bending strength values. For the TCO specimens, no value can be determined, as only two specimens broke in this extended edge area. These do not represent the distribution of edge strengths of the complete set of four specimens. The actual value is larger than 78.5 N/mm², which was calculated using the test results of the two specimens.

Table 7: Calculation of the bending strength in the edge ablated area (mean values, standard deviation in brackets).

Specimens	number of specimens considered	B [mm]	h [mm] mean value	σ_{bth} [N/mm²]		k_{ea}		$\sigma_{bB} = \sigma_{eff}$ [N/mm²]	
TCO	2	1100	3.16	74.7	(7.7)	1.050	(0.001)	> 78.5	
PV CdTe	4	600	3.21	68.0	(5.9)	1.067	(0.001)	72.6	(6.3)
PV a-Si/μ-Si longitudinal	8	1100	3.14	69.2	(4.0)	1.051	(0.000)	72.7	(4.1)
PV a-Si/μ-Si transversal	8	1300	3.16	69.7	(1.3)	1.054	(0.000)	73.5	(1.4)

2.6. Influence of PV coating

While the majority of the uncoated TCO specimens failed in the interior of the surface area, all PV specimens broke near the edge. Weller and Tautenhahn (2011) have documented the same effect for 600 mm wide CIS type specimens. Moreover, the analysis of the stress distribution supports the assumption that the geometry of the PV specimens principally would cause failures in the interior of the surface area, too. Thus, edge ablation appears to weaken the glass surface and finally to reduce the bending strength of PV modules. The identical a-Si/μ-Si type specimens PV 1100 and PV 1300 tested in different orientations result in similar mean values for bending strength. The mean value of the overall bending strength of all the 16 specimens considered, 72.4 N/mm², is 7 % lower than the TCO specimens without PV coating taken from the same batch of the same glass manufacturer (see table 8). Focusing on the ablated edge area, the difference is larger than 7 %. Therefore, a reduction in the bending strength due to the PV coating of a similar dimension can be assumed. The PV coating and laser scribing processes have a less critical influence on the surface quality than edge ablation.

Table 8: Statistical evaluation of photovoltaic panes in four point bending. s: overall bending strength, ea: edge ablation area only.

Specimens	number of specimens considered	B [mm]	h [mm]	σ_{bB} [N/mm²] mean value		variation coefficient		f_k [N/mm²] = 5 % fractile	
				s	ea	s	ea	s	ea
Uncoated (a-Si/μ-Si superstrate with TCO)	4 (ea: 2)	1100	3.16	77.6	> 78.5	5.9 %		57.4	
PV a-Si/μ-Si	16	1100 or 1300	3.15	72.4	73.1	4.2 %	4.1 %	65.1	65.8
PV CdTe	4	600	3.20	71.2	72.6	8.5 %	8.6 %	46.3	46.9

Although the number of specimens considered, i. e. those with fracture origin between the bending rollers, actually is too small for statistical evaluation, table 8 includes a statistical evaluation in order to show the general ability of both PV products tested to meet the minimum bending strength value for float glass. The 5 % fractile serves as the characteristic value. It is based on logarithmic normal distribution and relates to 5 % breakage probability and a confidence interval of 95%. Even for the CdTe type specimens, which exhibit the earlier fracture and particularly high variation, the characteristic value f_k exceeds the minimum characteristic bending strength of 45 N/mm². However, the results do not enable us to qualify the bending strength of the two PV products tested. Due to the generally large scattering of glass, a large number of specimens must be tested.

In conclusion, the overall bending strength values can serve as a conservative approach both for the unmeasured strength of the coated surface area and for the strength of the edge ablation area, which was determined to be higher.

2.7. Suitability of the modified test with extended specimen width

Extended specimen width results in reduced maximum stress at the edge and lessens the focus of the four point bending test method on the edge. Along with the typically high quality edge finish of the PV specimens, there are basically more failures in the interior of the surface area than at the edges in spite of the low stress level leading to fracture of float glass. In contrast to 360 mm wide thermally toughened glass specimens, critical defects within the whole test surface area account for breakage due to the more uniform stress development. In practice, the PV specimens nevertheless show fracture origins predominantly near the edge. This is due to the edge ablation process reducing the bending strength in this area. The modified test proved suitable to determine the bending strength of the coated substrate or superstrate glass used in PV thin-film modules. As a simplified approach for confirmation purposes, the evaluation procedure for the overall bending strength can be used to determine one global strength value. The standard evaluation procedure should be extended to incorporate the size effect for extended specimen widths. No modification of factor $k_s = 1$ is necessary for the analyzed specimen geometries. This global strength value underestimates bending strength both in the coated surface area and in the ablated edge area, because the ablated edge as a weak point coincides with the maximum stresses at the edge and thus provides sufficient safety.

3. Residual strength of glass-glass PV modules

3.1. PV products and test method

Residual strength or residual load-bearing capacity is the ability of a glazing structure, once broken, to remain securely in the fixing without any large pieces of glass falling down. It must continue to carry a minimum load level over a sufficient period, typically of one or several days, until the damage is detected and secured. Residual strength can only be verified experimentally. However, there are no harmonized test methods to prove residual strength. Based on previous schedules by various German building authorities, a test concept was developed to analyze three common PV module configurations in comparison with laminated safety glass of identical dimensions and sections. These served as reference, because there is no other general benchmark for residual strength. Moreover, the use of innovative thin-glass was considered.
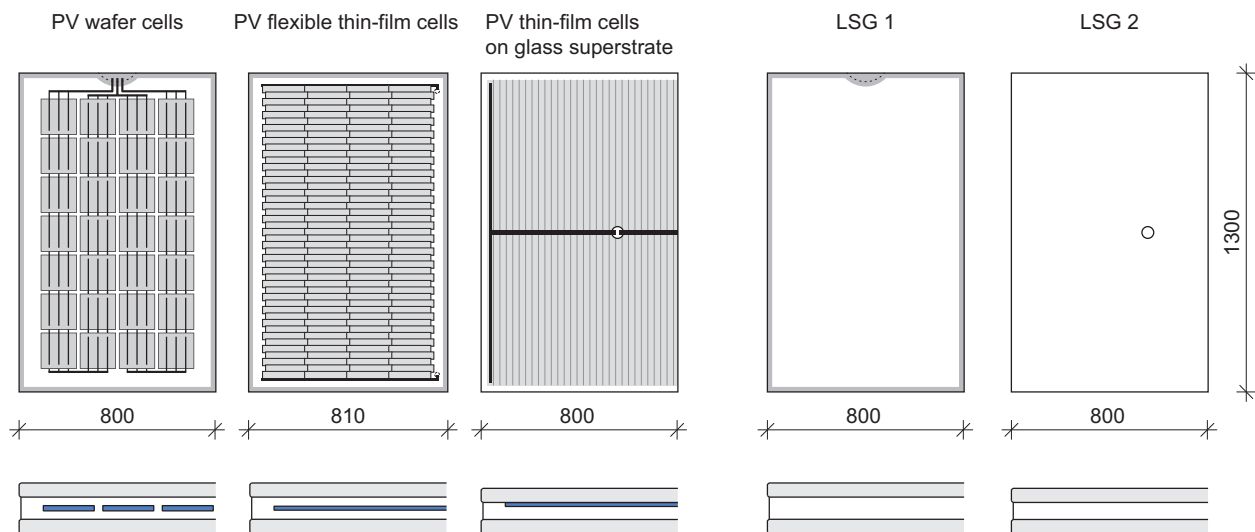
Fig. 10 View and section (not to scale) of PV module samples and laminated safety glass (LSG) references. PV superstrate module: back view. All others: front view.

The PV module types tested include

- interconnected 3 busbars polycrystalline silicon wafer cells integrated in a 1.0 mm polyvinyl butyral (PVB) interlayer between
  a) float glass panes 2 x 3.2 mm or, alternatively, between
  b) thin glass panes 2 x 2.1 mm
- adhesively connected flexible CIS on polyimide substrate cells affixed to a carrier mat and integrated in a 1.0 mm thermoplastic polyolefin (TPO) interlayer between thermally toughened glass panes 2 x 3.2 mm
- a-Si/μ-Si thin-film on glass superstrate; float glass 2 x 3.2 mm; 0.76 mm PVB interlayer.

The viscoelastic behavior of the polymeric interlayer materials had been analyzed using dynamic mechanical analysis (DMA) in the tension mode at frequencies between 0.5 and 10.0 Hz and temperatures from -50 to +100 °C. The PVB foils of two different manufacturers showed very similar thermomechanical behavior with a typical drastical loss in stiffness at temperatures larger than room temperature. In contrast, the stiffness of the TPO material

was less temperature dependent and decreased continuously with increasing temperature without a distinct drop. Up to room temperature, TPO was softer than PVB and at temperatures above 26 °C it was stiffer (Hemmerle 2015).

Shear tests, which were carried out at room temperature on small samples cut from laminated modules, also resulted in a lower stiffness of the TPO interlayer in comparison with PVB. Moreover, the interfaces between PVB and the rear side of the silicon wafer cells as well as between the self-adhesive rear side of the CIS cells and the carrier mat were the weak point in adhesion (Weller and Hemmerle 2014).

Since the embedded wafer and flexible cells need an interlayer on both sides, which add up to a higher total thickness than the PV thin-film on glass superstrate modules, two different types of LSG samples without PV cells and with different PVB thicknesses served as reference:

- LSG 1: float glass 2 x 3.2 mm; 1.00 mm PVB interlayer for wafer cells samples
- LSG 2: float glass 2 x 3.2 mm; 0.76 mm PVB interlayer for the PV thin-film on glass superstrate samples

The PV module manufacturers produced the LSG reference samples using the same interlayers as for the PV modules. Testing was carried out on full size components in order to incorporate effects of the cell interconnections and included four different types of fixing. This paper only covers linear support on four sides using a conventional façade system as supporting construction.

Three worst-case temperature and load scenarios were defined (see table 9). The maximum load occurs as pressure caused by combined wind and snow loads in winter. As the interlayers' tensile strength decreases with higher temperatures and increases with lower temperatures, testing at room temperature provides conservative results for the snow-covered winter scenario. The 100 % load level of 0.65 kN/m^2 corresponds to half the load-bearing capacity of the non-broken samples comprising 2 x 3.2 mm float glass.

Table 9: Load scenarios.

Test scenario	Loading condition	Temperature	Test load	Test time
winter	pressure	+23 °C	100 %	≥ 72 h
transitional	suction	+50 °C	50 %	≥ 24 h
summer	suction	+70 °C	32 %	≥ 24 h

The maximum temperature as worst case for the interlayers occurs in summer. In this case, maximum PV module temperatures correlate with wind suction as relevant design load. A test temperature of +70 °C over the entire test time was defined. Under German climate conditions, building integrated PV modules exceed this temperature on a few days a year, but only for a short daily period. As weather data analyses by Wellershoff (2009) show, there are no heavy storms on sunny days. Thus, the summer load level was reduced to 32 % or 0.21 kN/m^2. The intermediate scenario combines a module temperature of 50 °C and a 50 % load level equal to 0.325 kN/m^2. This scenario refers to winter days without snow cover or the transitional seasons.

Three samples per sample type and parameter were tested. Small sandbags were used as load to ensure a uniform distribution. Center deflection and failure served as main indicators for residual strength. The benchmarks were a test time of three days without failure for the high-pressure load scenario and 24 hours for the increased temperature scenarios.

In order to analyze the influence of aging on the residual strength, a-Si/μ-Si thin-film on glass superstrate samples and modules with flexible CIS cells were tested in the winter and transitional scenario after sequential exposure to 1000 hours of damp heat, 50 thermal cycles and 10 humidity-freeze cycles according to EN 61646. This aging scenario was not supposed to simulate a particular period of field operation, but to put the modules in a sufficiently aged state in order to generally analyze the sensitivity of the residual strength results to aging.

Three samples in parallel were mounted horizontally to a test rig (see figure 11b). In order to simulate wind suction and increased sample temperature, the test rig was placed in a heated temperature chamber and the support structure was mounted upside down to apply the sandbags on the rear side. Before the test load was applied, the samples were damaged. For this purpose, various damaging procedures had been tried. For the samples consisting of float glass and thin glass, dropping a 4.1 kg steel ball from a height of 2.5 m on the center of the front glass provided reproducible fracture patterns with cracks running to all edges of both glass panes. The thermally toughened glass panes of the CIS PV modules were damaged using a prick punch.

Fig. 11a) Typical fracture pattern of the a-Si/μ-Si superstrate modules (front view) before load application; b) Test rig for the winter scenario at room temperature.

3.2. Results

Figure 12a) shows the measured center deflections in the winter scenario at room temperature. The ball drop and the subsequent application of the sandbags caused a steep initial slope. The curves stabilize at 15 minutes test time, but the deflections keep increasing constantly. None of the samples failed within three days. In comparison with the laminated safety glass reference (LSG 2 with 0.76 mm PVB), the PV thin-film on glass superstrate modules showed 13 to 14 % less deflection, which indicates a better residual resistance. LSG 1 with thicker PVB (1.0 mm) performs better than LSG 2. The PV modules with embedded wafer cells and float glass had 20 to 25 % lower center deflections than the LSG 1 reference. The wafer modules with thin glass exhibited finer fracture patterns than the float glass modules, but not much of a difference in deflection. The center deflections of the PV modules with flexible cells, however, are considerably lower, in spite of their thermally toughened glass breaking into small particles, which normally – without the integrated cells – cannot provide residual strength. Thus, the integration of all three types of PV cells improved the residual resistance.
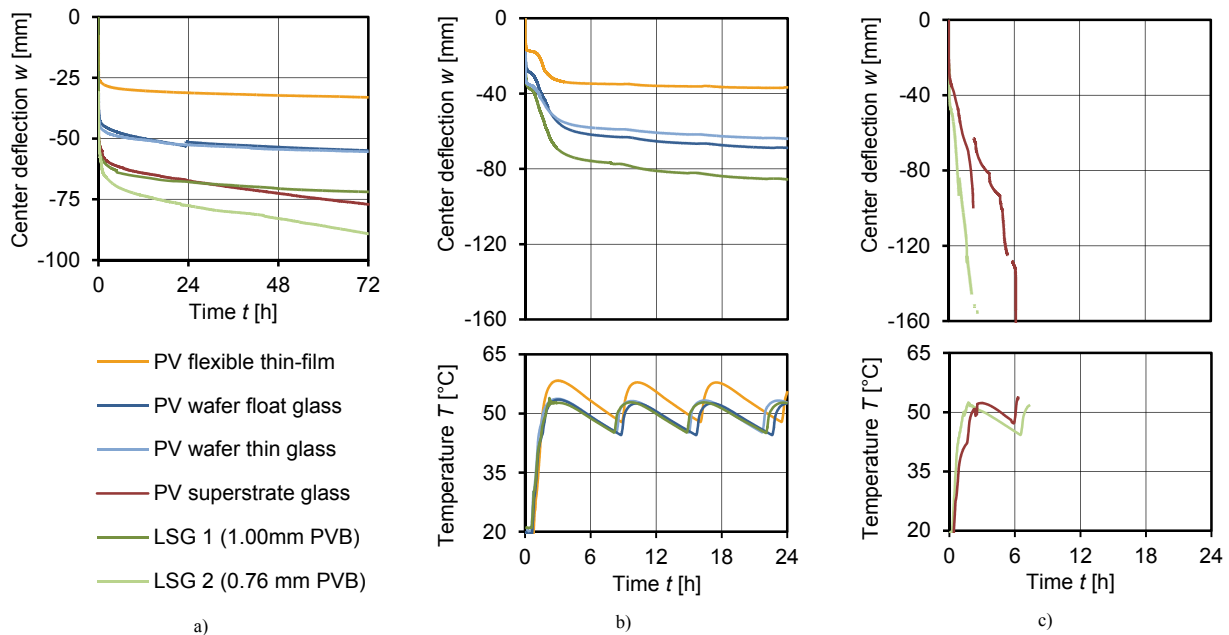
Fig. 12 Mean values of the measured center deflections a) in the winter scenario = pressure load 0.65 kN/m^2 at room temperature, b) and c) in the transitional scenario = suction load 0.325 kN/m^2 at +50 °C.

The results of the transitional scenario at an increased temperature of +50 °C and a load reduced to 50 % showed the same tendency, but deflections increased. Related to the lower temperature dependency of the TPO interlayer, the PV modules with flexible CIS cells exhibited less increase. The interlayer thickness emerged as crucial parameter for the samples using PVB: the PV and LSG 2 samples with only 0.76 mm PVB layer failed as soon as the sample temperature reached +51 to +55 °C, whereas LSG 1 and the PV wafer modules comprising a 1.0 mm PVB layer endured the entire test time of 24 hours.

PV thin-film on glass superstrate modules, LSG 2 samples and PV CIS modules were tested in the summer scenario at a temperature of +70 °C and a load reduced to 32 % equating to 0.21 kN/m^2. All PV superstrate modules and

LSG 2 samples with only 0.76 mm PVB layer failed as soon as the sample temperature reached +63 to +72 °C. As in the transitional scenario, the average failure temperatures of the PV thin-film on glass superstrate modules were 1 K lower than those of the LSG 2 samples. The CIS PV modules showed higher deflections than in the transitional scenario, but did not fail within 24 hours at an average module temperature of +72 °C.

The aged thin-film silicon modules were subject to increased breakage within the PV layer. Thus, the steel ball knocked out larger pieces of broken glass and left a buckle at the point of impact. Generally, the center deflection was greater than with unaged modules, but still no sample failed in the winter scenario. In the transitional scenario, again all samples failed at temperatures between +53 and +54 °C. The deflection of the PV modules with flexible CIS cells, however, did not increase after aging. Most modules had some delamination near the edges, but only one module with severe delamination along the entire edge failed in the transitional scenario.

An increased load until failure after the end of the tests lead to different failure modes of unaged PV superstrate glass modules and LSG 2: while the LSG 2 samples fell down as a whole, the PV modules broke in two due to the PVB interlayer tearing. The aged PV superstrate modules, however, did not go to pieces under ultimate load, but fell down as a whole.

3.3. Evaluation of module configurations

Evaluating the results, all PV module configurations showed an improved or equivalent residual strength compared to laminated safety glass.

a)   b)   c)
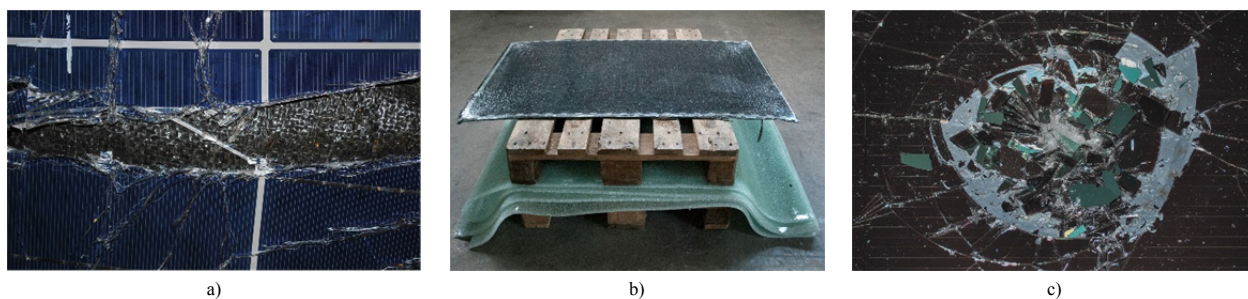
Fig. 13 Post breakage characteristics of a) PV wafer cell modules at +50 °C, b) PV modules with flexible thin-film cells in contrast to laminated safety glass made of thermally toughened glass without integrated PV cell layer and c) PV thin-film on glass superstrate modules.

Interconnected wafer cells reinforce the broken laminate, because the soldered interconnectors support tensile forces (see figure 13a)). Thus, deflection reduced by 20 to 25 % at room temperature as well as at +50 °C. Even if increased warming of the PV modules due to the cells' solar absorptance during operation is taken into account, the overall effect of the PV integration on the residual load-bearing capacity remains positive. The lower adhesion of PVB to the rear side of the cells than to glass seems to have no negative influence. In terms of residual strength, 2.1 mm thin glass is comparable to 3.2 mm float glass. Using thicker (PVB) interlayers improves residual strength.

Adhesively connected flexible PV cells significantly stiffen the broken laminate, because they form an additional layer with good tensile properties. As figure 13b) illustrates, conventional laminated safety glass made of thermally toughened glass panes becomes flexible once broken and does not provide any residual load bearing capacity. Thus, the integrated PV cells do not only improve post breakage behavior, but are the primary cause of residual strength. In principle, these findings also apply to other PV technologies using flexible films to be integrated in laminated glass, e. g. organic based photovoltaics.

The critical point of the PV thin-film on glass modules is mechanical failure within the PV layer (see figure 13c)), which increased after aging; and the resulting larger number of glass splinters associated with the risk of falling down when the PV coated glass pane is the impacted side and faces down (here: in the wind suction scenarios). However, splinter size and quantity seem to be non-dangerous. A reduction in deflection by 13 to 14 % compared to laminated safety glass is attributed to the cross-bus along the transverse axis. This tin-coated copper strip connects the outmost cells with the junction box in the center. Different cross-bus layouts available in other PV thin-film modules may result in different reinforcing effects. Tear resistance of the interlayer was found an essential property related to residual strength of PV thin-film on glass modules. In general, residual strength is evaluated equivalent to laminated safety glass.

3.4. Recommendations on approval and testing

As the integration of all three PV cell types proved to enhance or at least not impair residual load-bearing behavior of laminated glass, standard module configurations can be classified to provide the same residual strength performance as laminated safety glass, if the interlayer material is approved for use in laminated safety glass.

Thus, only special designs require individual approval of residual strength. For experimental verification purposes, the winter scenario applying a test load corresponding to 50 % of the design wind and snow load (or a minimum of 0.5 kN/m^2) at room temperature has proved itself. If the mechanical properties of the interlayer material used significantly change at temperatures larger than room temperature, additional testing in an increased temperature and reduced load scenario is recommended and specified in the following.

Laminated safety glass with PVB is the only acknowledged residual strength benchmark. Usually, the minimum PVB thickness to guarantee sufficient residual load bearing capacity is 0.76 mm or thicker. The tests carried out in the transitional scenario showed that the tensile strength limit of the 0.76 mm PVB interlayer was exceeded at +50 °C and half the test load. Thus, this load temperature configuration appears to be appropriate, while the summer scenario combining 32 % of the test load and a temperature of +70 °C is too severe. Taking into account that PV modules may reach 5 to 6 K higher temperatures than transparent laminated safety glass (Hemmerle 2015), an increase of testing temperature by 10 K provides sufficient safety for residual strength testing. As a result, testing at increased temperature should be carried out at a module temperature of +60 °C at a load corresponding to 25 % of the design wind load, but not less than 0.25 kN/m^2.

Further investigations on PV thin-film on glass substrate and superstrate glass modules focusing on the potential danger of broken glass pieces falling down would be of interest and should consider aging effects. In this regard, tests on small samples like the ones suggested in EN 14449, annex C may be suited.

4. Conclusions

The systematic and material-based examination of the post-breakage behavior of photovoltaic modules provided by this research can help to reduce the need for additional testing and approval, and thus facilitate the use of building-integrated photovoltaics. Based on these results, the standard module configurations tested provide sufficient residual load-bearing capacity, which is a fundamental property of laminated safety glass.

Using full-size photovoltaic-coated glass panes as specimens in four point bending represents a simple and feasible test method in order to determine and confirm the characteristic bending strength of thin-film superstrate or substrate modules. The altered dimensions of the specimens, with respect to the existing testing standard, requires modification of the evaluation procedure related to the size effect of glass strength.

Acknowledgements

References

Blank, K., Grüters, H., Hackl, K.: Contribution to the size effect on the strength of flat glass. In: Glastech. Ber. 63, No. 5, 1990, pp. 135-140.

Blank, K., Dürkop, D., Durchholz, M.; Grüters, H., Helmich, G., Senger, W.: Strength tests of flat glass by means of four-point bending. In: Glastech. Ber. Glass 67, No. 1, 1994, pp. 9-15.

DIBt Deutsches Institut für Bautechnik: Hinweise für die Herstellung, Planung und Ausführung von Solaranlagen. Berlin: Juli 2012

Dietrich, S.: Forschungsprojekt MecModule. Teilvorhaben Mechanisches Verhalten und Lebensdauer großflächiger Photovoltaikmodule. Abschlussbericht. Halle: Fraunhofer-Center für Silizium-Photovoltaik CSP, 2013.

EN 572-1: Glass in building – Basic soda lime silicate glass products – Part 1: Definitions and general physical and mechanical properties. 2012.

EN 1288-1: Glass in building. Determination of the bending strength of glass – Part 1: Fundamentals of testing glass. 2000.

EN 1288-2: Glass in building. Determination of the bending strength of glass – Part 3: Test with specimen supported at two points (four point bending). 2000.

EN 1288-3: Glass in building. Determination of the bending strength of glass – Part 2: Coaxial double ring test on flat specimens with large test surface areas. 2000.

EN 1288-5: Glass in building. Determination of the bending strength of glass – Part Part 5: Coaxial double ring test on flat specimens with small test surface areas. 2000.

EN 14449: Glass in building – Laminated glass and laminated safety glass – Evaluation of conformity/Product standard. 2005.

EN 61646: Thin-film terrestrial photovoltaic (PV) modules – Design qualification and type approval. 2008.

EN ISO 12543-1: Glass in building – Laminated glass and laminated safety glass – Part 1: Definitions and description of component parts. 2011.

Hemmerle, C.: Photovoltaik in der Gebäudehülle. Wertung bautechnischer Anforderungen. Photovoltaics in Building Envelopes. Evaluation of Structural Requirements. PhD thesis, Technische Universität Dresden, 2015.

Weller, B.; Hemmerle, C.: Forschungsprojekt BIPV – Gebäude- und elektrische Systemintegration. Teilvorhaben Baurecht und Prüfverfahren. Schlussbericht. Dresden: Institute of Building Construction of the Technische Universität Dresden, 2014.

Weller, B.; Tautenhahn, L.: Bestimmung der Biegezugfestigkeit im Vierschneidenverfahren in Anlehnung an die DIN EN 1288-3, Bauteil: beschichtete und unbeschichtete Einzelscheiben aus Floatglas. Prüfbericht Nr. 2011/282, 17.05.2011. Institute of Building Construction of the Technische Universität Dresden.

Wellershoff, F.: Nutzung der Verglasung zur Aussteifung von Gebäudehüllen. PhD thesis, RWTH Aachen, 2006.